

ORIGINAL REPORT OPEN ACCESS

Contrast Agent Uptake in Endolymphatic Sac and Duct: Inverse Relation to Endolymphatic Hydrops

Johannes Gerb^{1,2}  | Emilie Kierig² | Valerie Kirsch^{1,2,3} | Sandra Becker-Bense¹ | Rainer Boegle^{1,2} | Thomas Brandt^{1,2} | Marianne Dieterich^{1,2,3,4}

¹German Center for Vertigo and Balance Disorders, LMU University Hospital, LMU Munich, Munich, Germany | ²Department of Neurology, LMU University Hospital, LMU Munich, Munich, Germany | ³Graduate School of Systemic Neuroscience, LMU Munich, Munich, Germany | ⁴Munich Cluster for Systems Neurology (SyNergy), Munich, Germany

Correspondence: Johannes Gerb (johannes.gerb@med.uni-muenchen.de)

Received: 19 December 2024 | **Revised:** 20 February 2025 | **Accepted:** 25 February 2025

Funding: This work was supported by the Friedrich-Baur-Stiftung (FBS), the Graduate School of Systemic Neurosciences (GSN) which was funded by the German Research Foundation (DFG), the German Federal Ministry of Education and Research (BMBF) in connection with the foundation of the German Center for Vertigo and Balance Disorders (DSGZ; grant number 01 EO 0901). JG and MD were supported by the Deutsche Stiftung Neurologie (DSN; project 80766113), MD by the Deutsche Forschungsgemeinschaft (DFG, German Research Foundation) under Germany's Excellence Strategy (Munich Cluster for Systems Neurology: EXC 2145 SyNergy).

Keywords: endolymphatic duct | endolymphatic hydrops | endolymphatic sac | inner ear | Ménière's disease | vertigo | vestibular migraine | vestibulopathy

ABSTRACT

Objectives: Ménière's disease (MD) and vestibular migraine (VM) can be associated with endolymphatic hydrops (ELH). The differential role of the endolymphatic sac and duct (ES/ED) system for the development of ELH is poorly understood.

Methods: On 251 delayed, contrast-enhanced inner ear MRI (iMRI) datasets from neurotological patients and healthy control participants, we evaluated (1) the visibility of the ES/ED system using a novel semi-quantitative scale, and (2) the dimensions of ELH, calculated using volumetric local thresholding (VOLT). Afterwards, statistical analysis of ES/ED radiologic visibility in relation to the grade of ELH, the degree of clinical symptoms, and audiometric findings was performed.

Results: Patients were divided into an MD cohort ($n = 68$, 34 females, mean age 54.5 ± 14.8 years) and a VM cohort ($n = 67$, 42 females, 45.9 ± 15.5 years). The remaining datasets did not fulfill diagnostic criteria for definite diagnoses ($n = 64$, 27 females, mean age 51.3 ± 16.6) or were from healthy controls (HC; $n = 52$, 27 females, 49.0 ± 18.1 years). MD patients showed the lowest ES/ED-visibility scores on the affected side (ANOVA $F(172,2)$: 20.60, $p < 0.001$), while the ES/ED-visibility on the non-affected side in MD patients was still significantly lower than in VM and HC (ANOVA $F(172,2)$: 6.80, $p = 1.44 \times 10^{-3}$). The ES/ED-visibility score and ELH volume (determined by VOLT, in mm^3) correlated inversely (Spearman's rho: -0.32 , Fisher's $z = -0.34$, $p < 0.001$).

Conclusion: ES/ED radiologic visibility in iMRI is inversely associated with ELH volumes. Patients with MD show substantially decreased ES/ED visibility on the affected ear and (less pronounced) on the unaffected ear, while VM and HC exhibit normal ES/ED visibility.

Level of Evidence: 3.

1 | Introduction

Imaging of the inner ear fluid compartments by magnetic resonance tomography is a valuable research tool, which can

aid in the diagnosis of vestibular disorders [1, 2]. Intravenous admission of contrast agent (CA) after 4–5 h causes a CA enrichment within the perilymphatic fluid in contrast to the non-enriching endolymphatic fluid. This contrast allows the

This is an open access article under the terms of the [Creative Commons Attribution](https://creativecommons.org/licenses/by/4.0/) License, which permits use, distribution and reproduction in any medium, provided the original work is properly cited.

© 2025 The Author(s). *The Laryngoscope* published by Wiley Periodicals LLC on behalf of The American Laryngological, Rhinological and Otological Society, Inc.

visualization and quantification of endolymphatic hydrops (ELH), a common finding in Ménière's disease (MD) [3, 4]. However, ELH also occurs in other vestibular syndromes such as vestibular migraine (VM) [5–7], and might constitute a disease-related epiphenomenon rather than play a direct causative role in MD [8]. The degree of ELH can be graded semi-quantitatively or volumetrically [3, 9, 10].

Recently, the use of endolymphatic sac (ES) or duct (ED) imaging parameters in delayed contrast-enhanced MRI of the inner ear has been shown to allow clinical endotyping of MD, with many MD patients exhibiting a reduced CA uptake within these structures in 4h delayed inner ear MRI [11–13]. The endotypes defined by these radiographic surrogate markers (such as the angular trajectory of the vestibular aqueduct) often correlate with specific phenotypic features [14].

This finding is in line with histopathological studies showing distinct MD subtypes [15]. Physiologically, the ES/ED system plays an important role in endolymph homeostasis [16], but also in the inner ear immune response [17]. Impaired ES/ED function with reduced endolymphatic fluid resorption has therefore been postulated as a key factor for the development of ELH [18]. However, a quantitative proof of a direct relationship between in vivo ELH volume and ES/ED system integrity by imaging parameters is still lacking.

In the current study, we therefore aimed to (i) quantitatively analyze delayed post-contrast MRI visibility of the ES/ED system in patients with neurotological disorders such as MD and VM; (ii) investigate the relationship between ELH and ES/ED visibility; and (iii) correlate the inner ear MRI findings with clinical data.

2 | Materials and Methods

2.1 | Setting and Institutional Review Board Approval

All data was acquired at the Interdisciplinary German Center for Vertigo and Balance Disorders at Munich University Hospital (LMU Munich), Germany, between 2015 and 2020. Approval of the institutional review board of Ludwig-Maximilians university was obtained before the initiation of the study (no. 641-15). All participants provided informed oral and written consent in accordance with the Declaration of Helsinki and its later amendments before inclusion in the study.

2.2 | Study Population and Clinical Testing

Inner ear datasets ($n = 502$) from 251 patients who underwent iMRI for exclusion or verification of ELH were included. Exclusion criteria were neurological or psychiatric disorders, as well as any MR-related contraindications [19], poor image quality, or missing MR sequences. The diagnostic workup consisted of a thorough neurological and audiological workup (e.g., history-taking and clinical examination), a detailed neuro-orthoptic assessment (e.g., Frenzel glasses,

fundus photography and adjustments of the subjective visual vertical), as well as neurotological testing (video-oculography during bithermal caloric irrigation and head impulse testing, vestibular evoked myogenic potentials, pure tone audiometry). Clinical diagnosis of vestibular disorders was based on international diagnostic criteria by the Bárány Society. In their current version, these guidelines do not require ELH imaging for diagnosis; all patients were aware that ELH imaging was performed for research purposes. Patients filled out the Dizziness Handicap Inventory (DHI [20]), the Vertigo Symptom Scale (VSS [21]), the Migraine Disability Assessment (MIDAS [22]) and the Headache Impact Test (HIT-6 [23]).

2.3 | Delayed Intravenous Gadolinium-Enhanced MRI of the Inner Ear

Four hours after intravenous injection of a standard dose (i.e., 0.1 mmol/kg body weight) of gadobutrol (Gadovist, Bayer, Leverkusen, Germany), subjects underwent MR imaging in a whole-body 3 Tesla MRI scanner (Magnetom Skyra, Siemens Healthcare, Erlangen, Germany) with a 20-channel head coil. For assessing ES/ED visibility, a T2-weighted, three-dimensional, fluid-attenuated inversion recovery sequence (3D-FLAIR) was acquired (TR 6000 ms, TE 134 ms, TI 2240 ms, FOV $160 \times 160 \text{ mm}^2$, 36 slices, base resolution 320, averages 1, acceleration factor of 2 using a parallel imaging technique with a generalized auto-calibrating partially parallel acquisition (GRAPPA) algorithm, slice thickness 0.5 mm, acquisition time 15:08 min). For inner ear cisternography, a high-resolution, strongly T2-weighted, 3D constructive interference steady state (CISS) sequence of the temporal bones was performed (TR 1000 ms, TE 133 ms, FA 100° , FOV $192 \times 192 \text{ mm}^2$, 56 slices, base resolution 384, averages 4, acceleration factor of 2 using GRAPPA algorithm, slice thickness of 0.5 mm and acquisition time 8:36 min).

2.4 | ES/ED Visibility Scale

In order to quantify the visibility of the ES/ED system, we used a novel semi-quantitative 4-point rating scale (Figure 1). For grading, an axial slice from the 3D-FLAIR depicting the inner ear at midmodiolar height was selected, and the ED was followed in a caudal direction until the ES was identified. In this grading system, 0° stands for no visibility of the ES/ED complex (non-visualization). If the ES/ED system can be visually identified, its intensity is then compared to the PLS intensity in the vestibulum at midmodiolar level: in grade 1° , the ES/ED intensity is lower (hypo-enhancement); in grade 2° it is similar (iso-enhancement), and in grade 3° it is higher (hyper-enhancement, see Figure 1).

2.5 | ELH Assessment

Using a previously described semi-automatic ELH analysis pipeline (VOLT [10]), ELH volumes were calculated for each dataset. This method allows reproducible and objective volumetric ELH assessment and utilizes a combination of deep learning segmentation and three-dimensional local thresholding image analysis to calculate the amount of ELH fluid in mm^3 . Additionally,

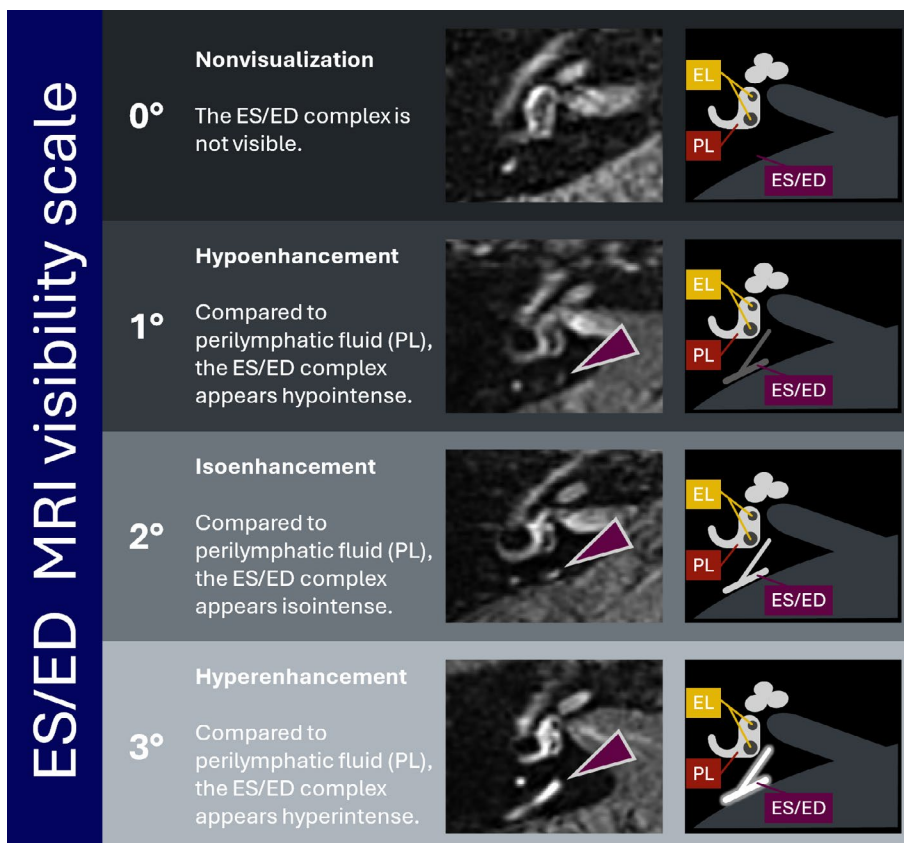


FIGURE 1 | ES/ED visibility scale for 4h post-contrast 3D-FLAIR images. At midmodiolar level on an axial slice of the inner ear, the ES/ED complex (marked in purple arrow) is identified and schematically depicted (right column). ES/ED image intensity is then compared to PL (marked in dark red) intensity: ES/ED 0° stands for no visibility (nonvisualization), ES/ED grade 1° stands for lower intensity (hypoenhancement), ES/ED grade 2° stands for similar intensity (isoenhancement), and ES/ED 3° stands for higher intensity (hyperenhancement). Note that the grade of endolymphatic hydrops, i.e., a potential increase of EL (marked in yellow), is not part of the ES/ED-scale. [Color figure can be viewed in the online issue, which is available at www.laryngoscope.com.]

clinical grading using the semi-quantitative scale from Baráth et al. [3] was performed by experienced neuroradiologists. In this grading system, ELH characteristics are assessed visually, and a set of image-based criteria is used to rate the degree of ELH.

2.6 | Statistical Analysis

For further statistical analysis, JASP 0.18.3 (jasp-stats.org) was used. Correlation between continuous variables was assessed using Spearman's rho, while binomial group comparisons were conducted using independent samples *t*-tests, and group comparisons for more than two groups were conducted using ANOVA with Tukey correction. *P*-values were controlled for multiple testing. In patients without a clinically leading ear (i.e., VM and HC cohort), a pseudorandom number generator [6] was used to assign “affected” and “non-affected” sides for cohort analyzes.

3 | Results

Of the 251 patients enrolled (mean age 50.3 ± 16.4 years, 130 females), the MD cohort consisted of 68 (34 females, mean age 54.5 ± 14.8), the VM cohort of 67 (42 females, mean age 45.9 ± 15.5), and the “vestibular healthy” controls of 52 patients (27 females, mean age 49.0 ± 18.1). The remaining datasets of 64

patients (27 females, mean age 51.3 ± 16.6) who did not fulfill the international diagnostic criteria for *definite* diagnoses, but only probable VM or MD, remained part of the general correlation analysis of ELH volume and ES/ED visibility but were excluded from the analysis of disease-associated effects.

3.1 | Clinical Details of MD and VM Cohort

The MD cohort had a higher mean age than the VM cohort (see Table 1 for details). No significant differences in disease duration were found. In vestibuloauditory testing, the MD cohort exhibited deficits on the affected side, while both groups had comparable findings on the non-affected side (affected and non-affected side were randomly assigned in the VM cohort, as described above). In the psychometric tests, the VM cohort typically described higher disease impact.

All MD patients were recommended betahistine treatment according to internal guidelines (recommended daily dosage: 72 mg). In case of symptom progression, some patients were treated with a higher daily dosage of up to 216 mg. At the time of MRI acquisition, 15 patients did not take any betahistine, 26 took lower dosages than recommended, 16 took the recommended dosage, and 5 took higher dosages. From the remaining six patients, no data was available. Betahistine dosage showed

TABLE 1 | Clinical findings in the MD and VM cohort.

	Unit	MD	VM	Welch's <i>t</i> -test
N (of which females)	—	68 (34)	67 (42)	—
Age	Years	54.5 ± 14.8	45.9 ± 15.5	<i>t</i> 3.31, <i>p</i> 1.20 × 10 ⁻³ , Cohen's <i>d</i> 0.57
Disease duration	Months	56.4 ± 59.1	69.0 ± 114.0	n. s.
Ipsilateral mean caloric excitability	%s	8.24 ± 7.51	11.31 ± 5.70	<i>t</i> -2.18, <i>p</i> 0.03, Cohen's <i>d</i> -0.46
Contralateral mean caloric excitability	%s	12.42 ± 8.60	11.93 ± 7.88	n. s.
Ipsilateral vHIT gain	—	0.82 ± 0.21	1.01 ± 0.30	<i>t</i> -3.07, <i>p</i> 3.73 × 10 ⁻³ , Cohen's <i>d</i> -0.74
Contralateral vHIT gain	—	0.86 ± 0.16	0.89 ± 0.15	n. s.
Ipsilateral low-frequency hearing loss	dB	43.26 ± 26.49	18.81 ± 14.64	<i>t</i> 5.80, <i>p</i> < 0.001, Cohen's <i>d</i> 1.14
Contralateral low-frequency hearing loss	dB	22.61 ± 16.59	16.81 ± 10.87	n. s.
MIDAS	Average grade (1: no migraine-related disability, 4: maximum disability)	2.62 ± 1.37	2.97 ± 1.24	n. s.
HIT-6	Average grade (1: no impact, 4: maximum impact of headaches on daily functioning)	1.90 ± 1.17	2.33 ± 0.99	<i>t</i> -2.31, <i>p</i> 0.03, Cohen's <i>d</i> -0.40
DHI	Points	34.88 ± 19.95	43.08 ± 22.00	<i>t</i> -2.20, <i>p</i> 0.03, Cohen's <i>d</i> -0.39
VSS	Points	29.50 ± 17.56	37.19 ± 21.37	<i>t</i> -2.13, <i>p</i> 0.04, Cohen's <i>d</i> -0.39

Note: Ipsilateral refers to the clinically affected side, and contralateral refers to the unaffected side. In VM patients, sides were assigned using a pseudorandom number generator. Note that the Migraine Disability Assessment (MIDAS) focuses on headache-associated disability, which often did not adequately represent VM patient symptomatology.

Abbreviations: DHI, Dizziness handicap inventory; HIT-6, headache impact test; MIDAS, Migraine disability assessment; VSS, Vertigo symptom scale; vHIT, video head impulse test.

no effect on ipsi- or contralateral ES/ED visibility, ipsi- or contralateral semiquantitative ELH grading, or ipsi- or contralateral volumetric (VOLT) ELH analysis (ANOVA: n. s.). None of the patients were undergoing diuretic treatment at the time of MRI acquisition, and none had undergone prior endolymphatic shunt surgery.

3.2 | ES/ED Visibility, ELH Volume and ELH Grading

In all inner ear datasets (*n* = 502), i.e., without any a priori filtering of diagnoses, ES/ED visibility score and ipsilateral ELH volume (determined by VOLT, i.e., an algorithm-based, volumetric volume calculation of inner ear fluid compartments) were inversely correlated: higher ELH volumes were associated with lower ES/ED visibility, and vice versa (Spearman's rho side: -0.32***, Fisher's *z* -0.34, *p* < 0.001). ES/ED visibility score and clinical semi-quantitative ELH grading were also inversely correlated (Spearman's rho: -0.21***, Fisher's *z* -0.21, *p* < 0.001). As expected, the VOLT volumes correlated positively with clinical grading (Spearman's rho: -0.42***, Fisher's *z* -0.45, *p* < 0.001).

ANOVA testing revealed significant differences after grouping by ES/ED visibility both for the ELH volumes (*F*(492,3) = 20.34, *p* < 0.001, mean ELH volume ES/ED 0°: 14.54 ± 6.36, ES/ED 1°: 12.15 ± 5.44, ES/ED 2°: 10.89 ± 3.95, ES/ED 3°: 10.11 ± 3.95) and for the clinical gradings (*F*(334,3) = 16.71, *p* < 0.001, mean ELH grade ES/ED 0°: 0.92 ± 0.84, ES/ED 1°: 0.52 ± 0.60, ES/ED 2°: 0.36 ± 0.47, ES/ED 3°: 0.34 ± 0.51; see Figure 2).

Independent of the clinical diagnosis, higher patient age correlated with lower ES/ED visibility (Spearman's rho -0.21***, Fisher's *z* -0.21, *p* < 0.001). Higher age additionally correlated with higher ELH volume determined by VOLT (Spearman's rho 0.10*, Fisher's *z* 0.10, *p* < 0.05), but not with the semi-quantitative visual grading (Spearman's rho n. s.). When analyzing individual patient datasets independent of diagnosis, ES/ED visibility score and ipsilateral ELH volume correlated inversely on both sides (Spearman's rho left side: -0.38***, Fisher's *z* -0.40, *p* < 0.001; right side: -0.24***, Fisher's *z* -0.25, *p* < 0.001). ES/ED visibility and contralateral ELH volume correlated as well, albeit with a smaller effect size (Spearman's rho left side: -0.26***, Fisher's *z* -0.27, *p* < 0.001; right side: -0.16*, Fisher's *z* -0.16, *p* < 0.05). ES/ED visibility score and ipsilateral clinical semi-quantitative

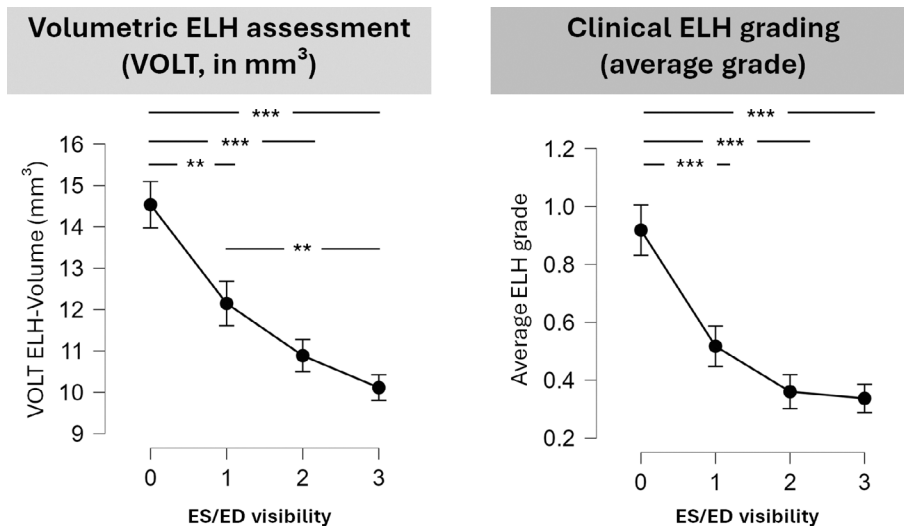


FIGURE 2 | Plots of ES/ED visibility and quantitative volumetric ELH assessment (volume in mm³, left) and clinical visual ELH grading (right) from 251 delayed contrast-enhanced inner ear datasets (502 individual inner ears). Lower ES/ED visibility exhibits a direct association with higher ELH volumes (calculated using VOLT), and with higher clinical ELH gradings (* = $p < 0.05$, ** = $p < 0.01$, *** = $p < 0.001$, Tukey-corrected ANOVA).

ELH grading correlated on both ears (Spearman's rho left side: -0.16^* , Fisher's $z -0.16$, $p < 0.05$; right side: -0.20^{**} , Fisher's $z -0.21$, $p < 0.01$). A correlation with the contralateral side could be observed (Spearman's rho left side: -0.17^{**} , Fisher's $z -0.18$, $p < 0.01$; right side: -0.14^* , Fisher's $z -0.15$, $p < 0.05$). The VOLT volumes correlated well with the ipsilateral clinical grading (Spearman's rho left side: -0.29^{***} , Fisher's $z -0.30$, $p < 0.001$; right side: -0.33^{***} , Fisher's $z -0.34$, $p < 0.001$), and were not affected by contralateral ELH (Spearman's rho with contralateral side: n. s.).

Patients with unilateral tinnitus showed ipsilaterally reduced ES/ED visibility (Welch's t -test ipsilateral ES/ED visibility: $t = 1.83$, $p = 0.03^*$, contralateral ES/ED visibility: $t = 1.26$, $p = 0.11$), while patients with bilateral tinnitus had higher ES/ED visibility on both sides (Welch's t -test ipsilateral ES/ED visibility: $t = -2.11$, $p = 0.02^*$, contralateral ES/ED visibility: $t = -1.97$, $p = 0.03^*$). Patients with unilateral aural fullness showed reduced ES/ED visibility on both sides (Welch's t -test ipsilateral ES/ED visibility: $t = 2.90$, $p = 2.31 \times 10^{-3**}$, contralateral ES/ED visibility: $t = 2.38$, $p = 9.69 \times 10^{-3**}$), while patients with bilateral aural fullness exhibited a higher ES/ED visibility on both sides (Welch's t -test ipsilateral ES/ED visibility: $t = -1.47$, $p = 0.08$, contralateral ES/ED visibility: $t = -1.31$, $p = 0.10$). Migraine symptoms were typically associated with bilaterally high ES/ED visibility, e.g., for headache (Welch's t -test ipsilateral ES/ED visibility: $t = -4.01$, $p = 5.04 \times 10^{-5***}$, contralateral ES/ED visibility: $t = -2.73$, $p = 3.57 \times 10^{-3**}$), and phono/photophobia: (Welch's t -test ipsilateral ES/ED visibility: $t = -1.46$, $p = 0.07$, contralateral ES/ED visibility: $t = -1.64$, $p = 0.05^*$). No linear correlation between ES/ED visibility and respective ipsilateral low- and high-frequency peripheral-vestibular function was observable (ES/ED and ipsilateral caloric excitability: n. s.; ES/ED visibility and ipsilateral vHIT gain: n. s.), but ES/ED visibility showed a highly significant negative correlation with ipsilateral low-frequency hearing impairment (Spearman's rho -0.27 , $p = 5.33 \times 10^{-3}$, Fisher's $z -0.28$). No linear association between ES/ED visibility and the psychometric tests (DHI, VSS, MIDAS, HIT-6) was found.

3.3 | Disease-Related Effects

In patients with MD, "affected" refers to the clinically leading ear, and "non-affected" refers to the opposite ear. In patients presenting without a leading clinical side and in the HC cohort, a pseudorandom number generator was used to assign "affected" and "non-affected" sides.

The ES/ED-score correlated well with the clinical diagnosis: MD patients showed the lowest scores on the affected side (ANOVA $F(172,2)$: 20.60, $p < 0.001$, mean score MD: 0.81 ± 1.08 ; VM: 1.91 ± 1.10 ; HC: 1.93 ± 1.19), while the ES/ED-visibility on the non-affected side in MD patients was still significantly lower than in VM and HC (ANOVA $F(172,2)$: 6.80, $p = 1.44 \times 10^{-3}$, mean score MD: 1.25 ± 1.18 ; VM: 1.87 ± 1.09 ; HC: 1.95 ± 1.15). The ELH volumes (calculated using VOLT) were the highest on the affected side in MD (ANOVA $F(164,2)$: 34.37, $p < 0.001$, mean score MD: 17.20 ± 7.23 ; VM: 11.42 ± 4.34 ; HC: 8.47 ± 2.44), while ELH volumes were comparable to VM (but still higher than HC) on the non-affected side (ANOVA $F(164,2)$: 6.18, $p = 2.58 \times 10^{-3}$, mean score MD: 11.61 ± 3.87 ; VM: 11.32 ± 4.73 ; HC: 8.79 ± 2.17). For the clinical ELH gradings, again, MD showed the highest ratings on the affected side (ANOVA $F(166,2)$: 52.00, $p < 0.001$, mean score MD: 1.22 ± 0.83 ; VM: 0.31 ± 0.39 ; HC: 0.18 ± 0.32) while a slight hydrops was seen on the non-affected side (ANOVA $F(166,2)$: 16.86, $p < 0.001$, mean score MD: 0.70 ± 0.60 ; VM: 0.26 ± 0.47 ; HC: 0.21 ± 0.33 , Figure 3).

4 | Discussion

In this study, a direct inverse relationship between ES/ED visibility and ELH severity in delayed, contrast-enhanced inner ear MRI could be demonstrated: the more pronounced the ELH, the lower the ES/ED contrast agent uptake. ES/ED visibility was asymmetrically decreased in MD patients, with the clinically affected side exhibiting the lowest visibility. ES/ED visibility was bilaterally high in VM and HC participants. Independent of the clinical diagnosis, higher patient age was

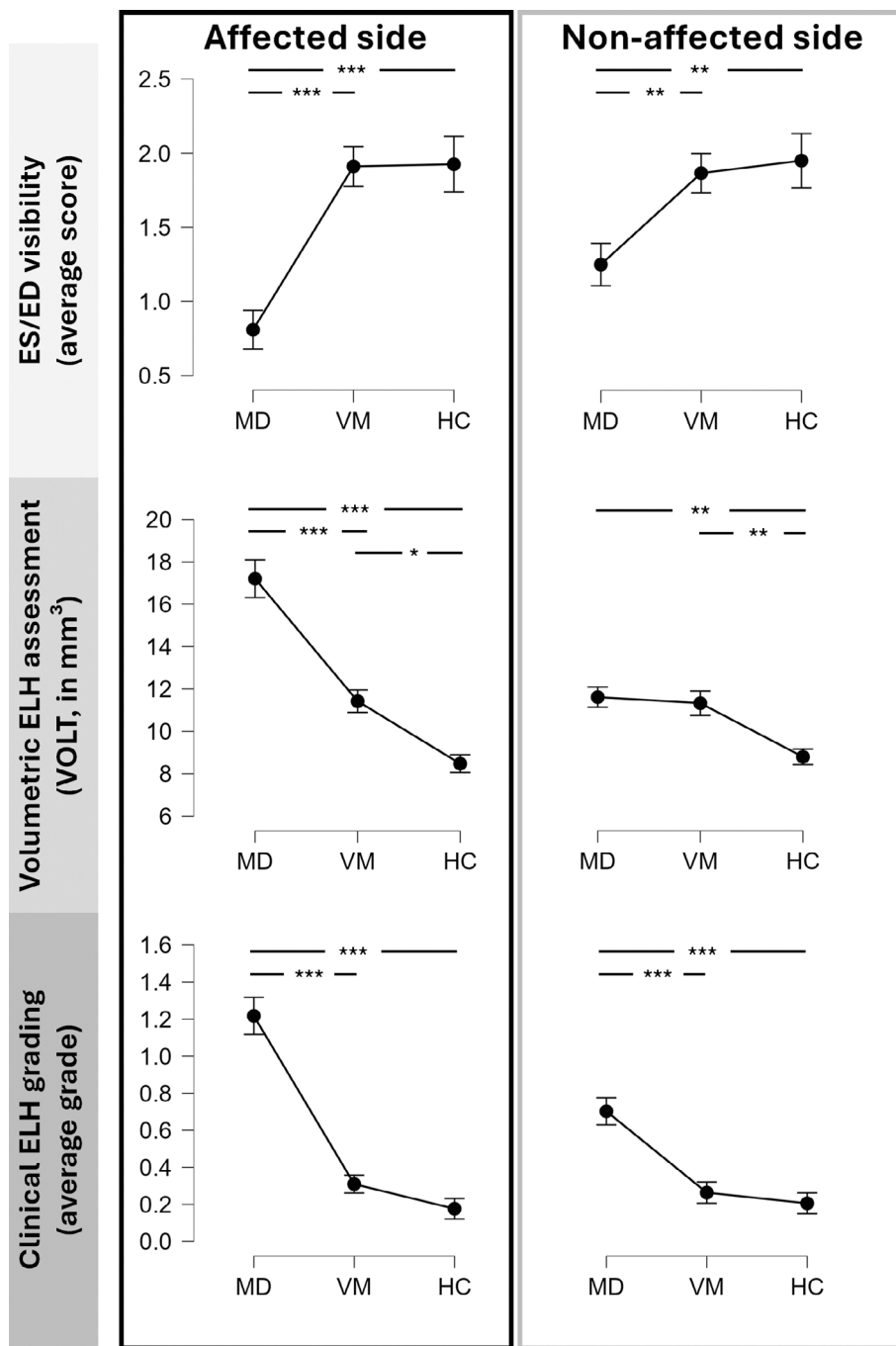


FIGURE 3 | Plots of ES/ED visibility, ELH volumes determined by VOLT⁶, and clinical visual ELH grading for affected (red rectangle) and non-affected patient side (blue rectangle), grouped for MD ($n=68$), VM ($n=67$) and vestibular healthy controls (HC, $n=48$). For VM without clinically leading sides and HC, assignment of affected and non-affected side was performed using a pseudorandom number generator. On the affected side, MD patients presented with the lowest average ES/ED visibility, the highest ELH volume, and the highest clinical ELH grading. On the non-affected side, MD patients showed typically slightly higher ES/ED visibility, lower ELH volumes, and lower ELH gradings. VM and HC presented with good ES/ED visibility, and the VM cohort exhibited mild, bilateral ELH only detectable using VOLT (*= $p<0.05$, **= $p<0.01$, ***= $p<0.001$, Tukey-corrected ANOVA).

associated with lower ES/ED visibility and higher ELH volumes. Lower ES/ED visibility was associated with MD-typical clinical signs and showed a strong correlation with low-frequency hearing deficits.

This approach, i.e., comparing detailed volumetric ELH analyzes with ES/ED post-contrast visibility analyzes, allows for an in vivo assessment of the endolymphatic fluid system.

Potentially, impairment of this fluid system, measured e.g., by analyzing post-contrast ES/ED visibility, could be used as a diagnostic radiographic marker in vestibular disorders. Earlier studies on the etiology and development of ELH proposed both hypersecretion of endolymphatic fluid and decreased resorption as pathophysiologically relevant factors. However, the microanatomy of the ES/ED complex and the in vivo fluid dynamics are only poorly understood [24]. While

peri-endolymphatic channels have been demonstrated in post-mortem temporal bone specimens [16, 25], in vivo investigations of their role in endolymph homeostasis are lacking. Based on our current findings, it can be stated that the ES/ED complex seems to play a crucial role in the development of ELH, although the exact pathomechanism remains uncertain. Here, multi-timepoint measurements visualizing the fluid dynamics (i.e., longitudinal flow, radial flow, dynamic flow, or no significant flow at all [26]) in the ES/ED complex could further illuminate the exact physiology. Additionally, higher resolution imaging approaches could aid in the exact localization of this CA uptake, i.e., revealing if these observations constitute “true” ES/ED signal intensity, or rather CA uptake in the aforementioned peri-endolymphatic channels.

It should be noted that this is the first study that correlated radiographic ES/ED signal intensity markers with detailed, volumetric measurements of the endolymphatic space in a large cohort of both vestibular healthy controls and patients (with and without ELH). Our findings of an inverse relationship between ES/ED visibility (either as “true” ES/ED visibility, or as an in vivo surrogate imaging marker of peri-endolymphatic channel CA uptake) and endolymphatic space, independent of clinical diagnosis or the presence of ELH, therefore imply a physiological relationship that might be modulated in MD. In general, this relationship, however, seems to be a sign of a basic, universal mechanism of inner ear fluid dynamics in both healthy and diseased inner ears.

Overall, these findings are in line with our previous findings of a symmetrical, low-grade ELH in VM, and an asymmetrical, higher grade ELH in MD [7]. Additionally, in the current study, the clinical symptoms described by patients correlated well with ES/ED visibility, independent of diagnosis: while unilateral, asymmetrical cochlear symptoms like aural fullness or tinnitus (i.e., symptoms typical for MD) were associated with an ipsilaterally decreased ES/ED visibility, bilateral and symmetrical cochlear symptoms (i.e., symptoms more commonly observed in VM) were associated with a bilateral, symmetric high ES/ED visibility. When analyzing symptoms typical for VM (e.g., phono-/photophobia, headache), again, a bilateral, symmetric high ES/ED visibility was observable. Therefore, a clear link between clinical symptomatology and ES/ED-visibility seems plausible. Based on these findings, a complete imaging-based diagnostic workup of vestibular disorders would therefore ideally include both ELH assessment and ES/ED visibility rating (using delayed, post-contrast MRI), paired with temporal bone morphology investigations (using high-resolution CT) for clinical endotyping of e.g., MD subtypes. These different modalities require adequate, inner-ear centered and geometry-preserving image co-registration [27]. As a simple “rule of thumb” classification, VM patients would typically present with (a) high bilateral ES/ED visibility, (b) no or low-grade ELH, and (c) normal temporal bone morphology, whereas MD patients would exhibit (a) severe ELH on the affected side, and no or low-grade ELH on the unaffected side, (b) low ES/ED visibility on the affected side, and medium ES/ED visibility on the contralateral side, and (c) ES/ED hypoplasticity or degeneration in temporal bone CT. Note that imaging alone cannot replace clinical reasoning, and should only be used to support clinical diagnoses.

The bilateral reduced ES/ED-visibility in MD patients, compared to the HC and VM cohorts, fits well with earlier observations by Bächinger et al. who showed that ES/ED hypoplasia or degeneration correlates with bilateral disease progression in a long-term MD cohort [28]. In a follow-up study, the authors could demonstrate lower ES/ED signal intensity specifically in the degenerative endotypes of MD [29]. The ES/ED-scale from our study could therefore provide a simple metric for the progression risk of MD to the contralateral ear in MD, which after 20 years may reach more than 40% [30, 31]. However, it should be noted that MD patients with a hypoplastic endotype [15] would exhibit inherently lower ES/ED visibility. Here, further research and longitudinal studies are necessary.

As a potential confounder of ELH volume analysis, the higher age of MD patients compared to VM patients needs to be considered. Earlier studies using volumetric analysis had shown an increase in endolymphatic volume in elderly healthy individuals [7, 32]. Other studies, which did not find a relationship between age and ELH, only employed semi-quantitative grading [33]. Potentially, small age effects may go undetected without the use of advanced, three-dimensional methods such as VOLT. Note that in the current analysis, age effects on ELH volume and ES/ED visibility were demonstrated independent of clinical diagnosis, i.e., also in healthy controls.

As a potential limitation, it should be noted that the ES/ED-visibility scale was tested on 3D-FLAIR images with the aforementioned sequence characteristics. Other sequences for ELH imaging exist, e.g., 3D inversion recovery (3D-IR [34]), or the HYDROPS- [35] and HYDROPSMi2-pipeline [36] which utilize two sets of 3D-FLAIR images finetuned to perilymphatic and endolymphatic fluid intensity. Due to the different imaging characteristics of these sequences, the applicability of the ES/ED scale for other methods of ELH visualization is currently unclear. However, similar to how VOLT (which was initially developed on FLAIR-images) could be shown to be applicable also in the HYDROPSMi2-pipeline [4, 37], an extension of the ES/ED scale to other ELH imaging pipelines could be possible and should be investigated in future studies.

5 | Conclusions

Assessment of ES/ED visibility in contrast-enhanced, delayed inner ear MRI using a novel semi-quantitative scale may support clinicians in the differentiation between episodic vertigo syndromes caused by MD or VM. Paired with endolymphatic hydrops imaging, ES/ED visibility assessment might additionally contribute to the understanding of the development and clinical course of inner ear disorders.

Acknowledgments

We thank Katie Göttlinger for copy editing the manuscript. Open Access funding enabled and organized by Projekt DEAL.

Conflicts of Interest

The authors declare no conflicts of interest.

References

1. N. V. Nagururu, A. Akbar, and B. K. Ward, "Using Magnetic Resonance Imaging to Improve Diagnosis of Peripheral Vestibular Disorders," *Journal of the Neurological Sciences* 439 (2022): 120300, <https://doi.org/10.1016/j.jns.2022.120300>.
2. M. Strupp, T. Brandt, and M. Dieterich, *Vertigo and Dizziness: Common Complaints*, 3rd ed. (Springer, 2023).
3. K. Baráth, B. Schuknecht, A. M. Naldi, T. Schrepfer, C. J. Bockisch, and S. C. A. Hegemann, "Detection and Grading of Endolymphatic Hydrops in Menière Disease Using MR Imaging," *American Journal of Neuroradiology* 35, no. 7 (2014): 1387–1392, <https://doi.org/10.3174/ajnr.A3856>.
4. S. Naganawa and T. Nakashima, "Visualization of Endolymphatic Hydrops With MR Imaging in Patients With Ménière's Disease and Related Pathologies: Current Status of Its Methods and Clinical Significance," *Japanese Journal of Radiology* 32 (2014): 191–204, <https://doi.org/10.1007/s11604-014-0390-4>.
5. W. Sun, P. Guo, T. Ren, and W. Wang, "Magnetic Resonance Imaging of Intratympanic Gadolinium Helps Differentiate Vestibular Migraine From Ménière Disease," *Laryngoscope* 127 (2017): 2382–2388, <https://doi.org/10.1002/lary.26518>.
6. S.-Y. Oh, M. Dieterich, B. N. Lee, et al., "Endolymphatic Hydrops in Patients With Vestibular Migraine and Concurrent Meniere's Disease," *Frontiers in Neurology* 12 (2021): 594481, <https://doi.org/10.3389/fneur.2021.594481>.
7. V. Kirsch, R. Boegle, J. Gerb, et al., "Imaging Endolymphatic Space of the Inner Ear in Vestibular Migraine," *Journal of Neurology, Neurosurgery, and Psychiatry* (2024): 334419, <https://doi.org/10.1136/jnnp-2024-334419>.
8. S. N. Merchant, J. C. Adams, and J. B. Nadol, "Pathophysiology of Ménière's Syndrome: Are Symptoms Caused by Endolymphatic Hydrops?," *Otology & Neurotology* 3 (2005): 5, <https://doi.org/10.1097/00129492-200501000-00013>.
9. R. Boegle, J. Gerb, E. Kierig, et al., "Intravenous Delayed Gadolinium-Enhanced MR Imaging of the Endolymphatic Space: A Methodological Comparative Study," *Frontiers in Neurology* 12 (2021): 647296, <https://doi.org/10.3389/fneur.2021.647296>.
10. J. Gerb, S. A. Ahmadi, E. Kierig, B. Ertl-Wagner, M. Dieterich, and V. Kirsch, "VOLT: A Novel Open-Source Pipeline for Automatic Segmentation of Endolymphatic Space in Inner Ear MRI," *Journal of Neurology* 267, no. Suppl 1 (2020): 185–196, <https://doi.org/10.1007/s00415-020-10062-8>.
11. D. Bächinger, N. N. Luu, J. S. Kempfle, et al., "Vestibular Aqueduct Morphology Correlates With Endolymphatic Sac Pathologies in Ménière's Disease—A Correlative Histology and Computed Tomography Study," *Otology & Neurotology* 40, no. 5 (2019): e548–e555, <https://doi.org/10.1097/MAO.0000000000002198>.
12. K. Xia, P. Lei, Y. Liu, et al., "Angular Trajectory of the Vestibular Aqueduct in a Cohort of Chinese Patients With Unilateral Ménière's Disease: Association With Other Imaging Indices and Clinical Profiles," *Biomedicine* 12, no. 9 (2024): 2008, <https://doi.org/10.3390/biomed12092008>.
13. L. M. H. Pont, M. T. P. M. Houben, T. O. Verhagen, et al., "Visualization and Clinical Relevance of the Endolymphatic Duct and Sac in Ménière's Disease," *Frontiers in Neurology* 14 (2023): 1239422, <https://doi.org/10.3389/fneur.2023.1239422>.
14. D. Bächinger, C. Brühlmann, T. Honegger, et al., "Endotype-Phenotype Patterns in Meniere's Disease Based on Gadolinium-Enhanced MRI of the Vestibular Aqueduct," *Frontiers in Neurology* 10 (2019): 303, <https://doi.org/10.3389/fneur.2019.00303>.
15. A. H. Eckhard, M. Zhu, J. T. O'Malley, et al., "Inner Ear Pathologies Impair Sodium-Regulated Ion Transport in Meniere's Disease," *Acta Neuropathologica* 137, no. 2 (2019): 343–357, <https://doi.org/10.1007/s00401-018-1927-7>.
16. C. K. Nordström, H. Li, H. M. Ladak, S. Agrawal, and H. Rask-Andersen, "A Micro-CT and Synchrotron Imaging Study of the Human Endolymphatic Duct With Special Reference to Endolymph Outflow and Meniere's Disease," *Scientific Reports* 10, no. 1 (2020): 8295, <https://doi.org/10.1038/s41598-020-65110-0>.
17. C. Kämpfe Nordström, N. Danckwardt-Lillieström, G. Laurell, W. Liu, and H. Rask-Andersen, "The Human Endolymphatic Sac and Inner Ear Immunity: Macrophage Interaction and Molecular Expression," *Frontiers in Immunology* 9 (2018): 3181, <https://doi.org/10.3389/fimmu.2018.03181>.
18. R. S. Kimura, "Experimental Blockage of the Endolymphatic Duct and Sac and Its Effect on the Inner Ear of the Guinea Pig. A Study on Endolymphatic Hydrops," *Annals of Otology, Rhinology, and Laryngology* 76, no. 3 (1967): 664–687, <https://doi.org/10.1177/000348946707600311>.
19. T. Dill, "Contraindications to Magnetic Resonance Imaging: Non-Invasive Imaging," *Heart* 94, no. 7 (2008): 943–948, <https://doi.org/10.1136/hrt.2007.125039>.
20. G. P. Jacobson and C. W. Newman, "The Development of the Dizziness Handicap Inventory," *Archives of Otolaryngology – Head & Neck Surgery* 116, no. 4 (1990): 424–427, <https://doi.org/10.1001/archotol.1990.01870040046011>.
21. L. Yardley, E. Masson, C. Verschuur, N. Haacke, and L. Luxon, "Symptoms, Anxiety and Handicap in Dizzy Patients: Development of the Vertigo Symptom Scale," *Journal of Psychosomatic Research* 36, no. 8 (1992): 731–741, [https://doi.org/10.1016/0022-3999\(92\)90131-k](https://doi.org/10.1016/0022-3999(92)90131-k).
22. W. F. Stewart, R. B. Lipton, J. Whyte, et al., "An International Study to Assess Reliability of the Migraine Disability Assessment (MIDAS) Score," *Neurology* 53, no. 5 (1999): 988–994, <https://doi.org/10.1212/wnl.53.5.988>.
23. M. Yang, R. Rendas-Baum, S. F. Varon, and M. Kosinski, "Validation of the Headache Impact Test (HIT-6™) Across Episodic and Chronic Migraine," *Cephalalgia* 31, no. 3 (2011): 357–367, <https://doi.org/10.1177/0333102410379890>.
24. H. Li, G. P. Rajan, J. Shaw, et al., "A Synchrotron and Micro-CT Study of the Human Endolymphatic Duct System: Is Meniere's Disease Caused by an Acute Endolymph Backflow?," *Frontiers in Surgery* 8 (2021): 662530, <https://doi.org/10.3389/fsurg.2021.662530>.
25. F. H. Linthicum, J. Doherty, P. Webster, and A. Makarem, "The Periductal Channels of the Endolymphatic Duct, Hydrodynamic Implications," *Otolaryngology and Head and Neck Surgery* 150, no. 3 (2014): 441–447, <https://doi.org/10.1177/0194599813516420>.
26. A. N. Salt, "Regulation of Endolymphatic Fluid Volume," *Annals of the New York Academy of Sciences* 942 (2001): 306–312, <https://doi.org/10.1111/j.1749-6632.2001.tb03755.x>.
27. J. Gerb, V. Kirsch, E. Kierig, et al., "Optimizing Spatial Normalization of Multisubject Inner Ear MRI: Comparison of Different Geometry-Preserving Co-Registration Approaches," *Scientific Reports* 15, no. 1 (2025): 6414, <https://doi.org/10.1038/s41598-025-90842-2>.
28. D. Bächinger, B. Schuknecht, J. Długaiczek, and A. H. Eckhard, "Radiological Configuration of the Vestibular Aqueduct Predicts Bilateral Progression in Meniere's Disease," *Frontiers in Neurology* 12 (2021): 674170, <https://doi.org/10.3389/fneur.2021.674170>.
29. D. Bächinger, N. Filidoro, M. Naville, et al., "Radiological Feature Heterogeneity Supports Etiological Diversity Among Patient Groups in Meniere's Disease," *Scientific Reports* 13, no. 1 (2023): 10303, <https://doi.org/10.1038/s41598-023-36479-5>.
30. M. Takumida, A. Kakigi, T. Takeda, and M. Anniko, "Meniere's Disease: A Long-Term Follow-Up Study of Bilateral Hearing Levels," *Acta Oto-Laryngologica* 126, no. 9 (2006): 921–925.

31. D. Huppert, M. Strupp, and T. Brandt, "Long-Term Course of Meniere's Disease Revisited," *Acta Oto-Laryngologica* 130, no. 6 (2010): 644–651.
32. M. Dieterich, T. Hergenroeder, R. Boegle, et al., "Endolymphatic Space Is Age-Dependent," *Journal of Neurology* 270, no. 1 (2023): 71–81, <https://doi.org/10.1007/s00415-022-11400-8>.
33. Y. Maeda, K. Kojima, S. Takao, R. Omichi, S. Kariya, and M. Ando, "Endolymphatic Hydrops on Magnetic Resonance Imaging May be an Independent Finding on Aging in Neurotologic Patients," *Otology & Neurotology* 44, no. 7 (2023): 737–741, <https://doi.org/10.1097/MAO.0000000000003945>.
34. S. Naganawa, H. Satake, M. Kawamura, H. Fukatsu, M. Sone, and T. Nakashima, "Separate Visualization of Endolymphatic Space, Perilymphatic Space and Bone by a Single Pulse Sequence; 3D-Inversion Recovery Imaging Utilizing Real Reconstruction After Intratympanic Gd-DTPA Administration at 3 Tesla," *European Radiology* 18, no. 5 (2008): 920–924, <https://doi.org/10.1007/s00330-008-0854-8>.
35. S. Naganawa, M. Yamazaki, H. Kawai, K. Bokura, M. Sone, and T. Nakashima, "Imaging of Ménière's Disease After Intravenous Administration of Single-Dose Gadodiamide: Utility of Subtraction Images With Different Inversion Time," *Magnetic Resonance in Medical Sciences* 11, no. 3 (2012): 213–219, <https://doi.org/10.2463/mrms.11.213>.
36. S. Naganawa, K. Suzuki, R. Nakamichi, et al., "Semi-Quantification of Endolymphatic Size on MR Imaging After Intravenous Injection of Single-Dose Gadodiamide: Comparison Between Two Types of Processing Strategies," *Magnetic Resonance in Medical Sciences* 12, no. 4 (2013): 261–269, <https://doi.org/10.2463/mrms.2013-0019>.
37. J. Gerb, V. Kirsch, B. N. Lee, et al., "P 74 Endolymphatic Hydrops of the Inner Ear in Patients With Vestibular Migraine and Concurrent Meniere's Disease—VOLT Algorithm Extension," *Clinical Neurophysiology* 137 (2022): e57–e58, <https://doi.org/10.1016/j.clinph.2022.01.105>.